Sugar in Two Steps

Hexose sugars are naturally abundant, but it is often useful to modify their structures for chemical and biochemical studies. Standard synthetic routes tend to be long and tedious and require multiple protection steps. **Northrup and MacMillan** (p. 1752, published online 12 August 2004) now describe a reaction sequence for generating the sugars from achiral aldehyde precursors in just two steps, thereby offering a convenient means of preparing diverse structural variants. In the first step, α-oxyaldehydes are dimerized with L-proline as the only source of asymmetry throughout the sequence. In the second step, an aldol addition-cyclization step is controlled by variation of solvent and Lewis acid to afford any of three stereoisomeric products (glucose, mannose, or allose), all in high yield and stereochemical purity.

Standing CO_2 on Its End

Understanding how plants reduce CO_2 to sugars, and facilitating attempts to mimic this chemistry, requires better insight into the specific binding geometry of CO_2 at metal centers. Synthetic chemists studying the problem usually start with metal complexes that coordinate CO_2 through the C atom, with one or both O atoms bent away from the metal. **Castro-Rodriguez *et al.*** (p. 1757) have prepared a U complex in which coordinated CO_2 remains linear and binds end-on to the metal through a single O atom. X-ray crystallography verified this unusual bonding geometry.

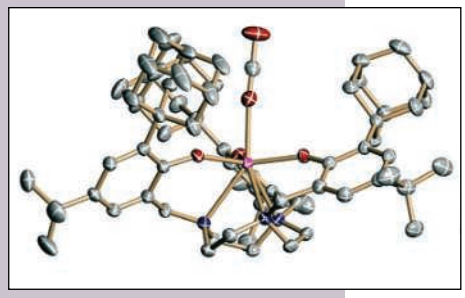

Disilyne Debut

Double and triple bonds are common in compounds of the first-row elements carbon, nitrogen, and oxygen. In contrast, the heavier main group congeners tend to form single-bonded networks instead, because repulsion by inner-shell electrons keeps the atoms too far apart for π-bonding. **Sekiguchi *et al.*** (p. 1755; see the Perspective by **West**) have managed to push two Si atoms close enough together to form a Si-Si triple bond. They reduced a brominated precursor in which the Si atoms bear very bulky side groups that help destabilize more conventional bonding options. X-ray crystallography revealed a bent geometry consistent with theoretical predictions that the silicon orbitals do not hybridize like those of carbon do in rigidly linear alkynes.

Early Oxygen History

Measurements of the three stable isotopes of oxygen in primitive meteorites that formed in the solar nebula indicate that the nebular gas had an initial enrichment in ^{16}O that was quickly depleted. Observations of molecular clouds indicate that ultraviolet radiation selectively dissociates $C^{17}O$ and $C^{18}O$, but not $C^{16}O$, which leaves the atomic oxygen gas in the interior of the cloud depleted in ^{16}O. **Yurimoto and Kuramoto** (p. 1763; see the Perspective by **Yin**) have developed a model to explain the meteoritical data using the astronomical observations. The oxygen isotopic differences developed in the molecular cloud via photodissociation. When the cloud collapsed into the solar nebula disk, the isotopic differences were transported to the inner disk by icy dust grains that evaporated when they neared the Sun.

Why the Ice?

The large, permanent ice sheets that presently occupy Antarctica began to form around 14 million years ago, when Earth entered a phase of global cooling. However, the climate processes that produced these changes, as well as the temporal relation between ice sheet growth and cooling, have remained obscure. **Shevenell *et al.*** (p. 1766) analyzed Mg/Ca ratios (a proxy for temperature), oxygen isotopes (which record a combination of temperature and seawater oxygen isotopic composition), and carbon isotopes (a proxy for atmospheric CO_2 concentrations) of benthic foraminifera from Southern Hemisphere marine sediments with ages between 15 and 13.2 million years. Deep-ocean cooling began roughly 60,000 years before ice sheet growth, and both of these processes happened during a period of atmospheric CO_2 increase. These findings suggest that factors other than radiative forcing, such as ocean heat transport, were key elements of this climate transition.

Damage-Free Dating

Many geologic boundaries reflect dramatic changes in species abundances or mark the origination of species. Thus, the accurate determination of their ages is essential for defining the pace of evolution. One of the best dating methods, based on the decay of U isotopes to Pb can be problematic if damaged parts of zircons, the primary uranium-bearing mineral, lose radiogenic Pb or incorporate older cores. **Mundil *et al.*** (p. 1760; see the News story by **Kerr**) used a recent method that strips out these damaged areas to refine the age of the end-Permian extinction and Permo-Triassic boundary. Their data on a sequence of ashes in two localities place the extinction at 252.6 million years ago, about 1 million years older than previously determined. The results support the conclusion that the extinction occurred within the limit of the method, just a few hundred thousand years.

Two Membranes, Two Fusion Mechanisms

Mitochondria, the powerhouses of the cell, are surrounded by a double membrane. Within the cell, mitochondria continually fuse with one another, but the mechanism by which their two membranes can faithfully fuse remains obscure. **Meeusen *et al.*** (p. 1747, published online 5 August 2004; see the Perspective by **Pfanner *et al.***) now present a cell-free assay that reconstitutes efficient mitochondrial fusion in

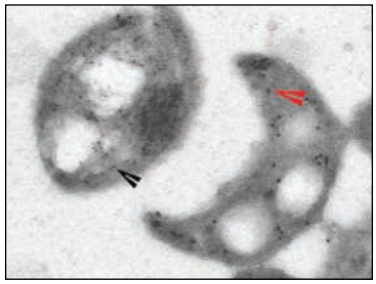

CONTINUED ON PAGE 1675

CREDITS: (TOP TO BOTTOM) CASTRO-RODRIGUEZ *ET AL.*; MEEUSEN *ET AL.*

Published by AAAS

3. P. P. Power, *Chem. Rev.* **99**, 3463 (1999).
4. M. Weidenbruch, *The Chemistry of Organic Silicon Compounds*, Z. Rappoport, Y. Apeloig, Eds. (Wiley, Chichester, UK, 2001), vol. 3, chap. 5.
5. E. Wiberg, *Lehrbuch der Anorganischen Chemie*, A. F. Holleman, E. Wiberg, Eds. (W. de Gruyter, Berlin, Germany, eds. 22 and 23, 1943).
6. J. Goubeau, *Angew. Chem.* **69**, 77 (1957).
7. P. Jutzi, *Angew. Chem. Int. Ed. Engl.* **14**, 232 (1975).
8. P. J. Davidson, M. F. Lappert, *J. Chem. Soc. Chem. Commun.* **1973**, 317 (1973).
9. R. West, M. J. Fink, J. Michl, *Science* **214**, 1343 (1981).
10. A. G. Brook, F. Abdesaken, B. Gutekunst, G. Gutekunst, R. K. Kallury, *J. Chem. Soc. Chem. Commun.* **1981**, 191 (1981).
11. (2,6-Tip_2-C_6H_3)PbPb(C_6H_3-2,6-Tip_2), where Tip is 2,4,6-*i*-Pr_3-C_6H_2-, is described in L. Pu, B. Twamley, P. P. Power, *J. Am. Chem. Soc.* **122**, 3524 (2000).
12. (2,6-$Dipp_2$-C_6H_3)SnSn(C_6H_3-2,6-$Dipp_2$), where Dipp is 2,6-*i*-Pr_2-C_6H_3-, is described in A. D. Philips, R. J. Wright, M. M. Olmstead, P. P. Power, *J. Am. Chem. Soc.* **124**, 5930 (2002).
13. (2,6-$Dipp_2$-C_6H_3)GeGe(C_6H_3-2,6-$Dipp_2$)$_2$ is described in M. Stender, A. D. Phillips, R. J. Wright, P. P. Power, *Angew. Chem. Int. Ed. Engl.* **41**, 1785 (2002).
14. P. P. Power, *Chem. Commun.* **2003**, 2091 (2003).
15. G. H. Robinson, *Acc. Chem. Res.* **32**, 773 (1999).
16. S. Nagase, K. Kobayashi, N. Takagi, *J. Organomet. Chem.* **611**, 264 (2000).
17. A. Sekiguchi, S. S. Zigler, R. West, *J. Am. Chem. Soc.* **108**, 4241 (1986).
18. R. Pietschnig, R. West, D. R. Powell, *Organometallics* **19**, 2724 (2000).
19. The reduction of $(^tBu_3Si)_2MeSiClSi{=}SiClSiMe(Si^tBu_3)_2$ with lithium naphthalene in THF has recently been reported (*28*). This contains an unstable product with a low field ^{29}Si NMR signal at $\delta = 91.5$ ppm, which was ascribed to a Si≡Si triple-bond resonance.
20. Crystals of **1** (100 mg, 0.087 mmol) and KC_8 (50 mg, 0.370 mmol) were placed in a glass tube and degassed. Dry oxygen-free THF (2 ml) was introduced by vacuum transfer and the mixture was allowed to warm from –78°C to room temperature overnight with stirring. The solution turned an intense green color. The solvent was replaced by hexane, and then the resulting potassium salt and graphite were filtered off in a glove box (a box equipped with gloves in which air- and moisture-sensitive compounds can be handled). After evaporation of the solvent, pentane was added and the solution was cooled at –30°C to give emerald green crystals of **2** (53 mg, 73%).
21. NMR of **2** ([D_6]benzene solution, ^1H) δ values (ppm): –0.01 (singlet, 4H), CH protons; 0.39 (singlet, 36H), $SiMe_3$ protons; 0.57 (singlet, 36H), $SiMe_3$ protons, 1.44 (doublet, 12H, spin-spin coupling constant $J = 6.0$ Hz, 12H), isopropyl methyl protons, 1.49 (septet, spin-spin coupling constant $J = 6.0$ Hz, 2H), isopropyl methyne proton. NMR (^{13}C) δ values: 5.1, 5.7, 8.9, 17.8, and 22.3. NMR (^{29}Si) δ values: –0.3, 0.0, 20.7, and 89.9. High-resolution mass spectrum: mass-to-charge ratio (*m*/*z*) calculated for $C_{34}H_{90}Si_{12}$ to be 834.4274, experimentally found to be 834.4275. Ultraviolet-visible spectrum (in hexane solution): λ_{max} [wavelength, molar extinction coefficient (ε)/dm^3 mol^{-1} cm^{-1}] 259, 10300; 328, 5800; 483, 120; and 690, 14.
22. M. Kira, T. Maruyama, C. Kabuto, K. Ebata, H. Sakurai, *Angew. Chem. Int. Ed. Engl.* **33**, 1489 (1994).
23. H. Sakurai, H. Tobita, Y. Nakadaira, *Chem. Lett.* **1982**, 1251 (1982).
24. An emerald green crystal (approximate dimensions, 0.30 by 0.15 by 0.15 mm) of **2** was used for the x-ray diffraction data collection on a Mac Science DIP2030K Image Plate Diffractometer with graphite-monochromatized Mo–K_α radiation ($\lambda = 0.71070$ Å). Cell constants and an orientation matrix for data collection corresponded to the monoclinic space group *C*2/*c*, with $a = 30.9620(11)$ Å, $b = 10.9060(2)$ Å, $c = 18.1170(7)$ Å, $\beta = 118.995(2)°$, $V = 5350.8(3)$ Å^3, four molecules per unit cell, formular weight 836.14, and calculated density 1.038 Mg/m^3. Data were collected at 120 K, θ range from 2.18° to 28.01°. There were 26,993 collected reflections (6412 unique, $R_{int} = 0.0290$); $R_1 = 0.0373$ for 5479 reflections with $I > 2\sigma(I)$, $wR_2 = 0.1096$ for all reflections. More crystallographic data are available at the Cambridge Crystallographic database, accession code and deposition no. CCDC 245523.
25. K. Kobayashi, S. Nagase, *Organometallics* **16**, 2489 (1997).
26. N. Takagi, S. Nagase, *Eur. J. Inorg. Chem.* **2002**, 2775 (2002).
27. M. Ichinohe, M. Toyoshima, R. Kinjo, A. Sekiguchi, *J. Am. Chem. Soc.* **125**, 13328 (2003).
28. N. Wiberg, W. Niedermayer, G. Fischer, H. Nöth, M. Suter, *Eur. J. Inorg. Chem.* **2002**, 1066 (2002).

29. Supported by a Grant-in-Aid for Scientific Research (Nos. 134078204, 16205008, and 16550028) from the Ministry of Education, Science and Culture of Japan, and Center of Excellence program. We thank S. Nagase for helpful discussions and advice.

Supporting Online Material
www.sciencemag.org/cgi/content/full/305/5691/1755/DC1
Tables S1 to S5

30 June 2004; accepted 2 August 2004

A Linear, O-Coordinated η^1-CO_2 Bound to Uranium

Ingrid Castro-Rodriguez, Hidetaka Nakai, Lev N. Zakharov, Arnold L. Rheingold, Karsten Meyer*

The electron-rich, six-coordinate tris-aryloxide uranium(III) complex [($(^{Ad}ArO)_3tacn)U^{III}$] [where $(^{Ad}ArOH)_3tacn$ = 1,4,7-tris(3-adamantyl-5-*tert*-butyl-2-hydroxybenzyl)1,4,7-triazacyclononane] reacts rapidly with CO_2 to yield [($(^{Ad}ArO)_3tacn)U^{IV}(CO_2)$], a complex in which the CO_2 ligand is linearly coordinated to the metal through its oxygen atom (η^1-OCO). The latter complex has been crystallographically and spectroscopically characterized. The inequivalent O–C–O bond lengths [1.122 angstroms (Å) for the O–C bond adjacent to uranium and 1.277 Å for the other], considered together with magnetization data and electronic and vibrational spectra, support the following bonding model: $U^{IV}{=}O{=}C^{\bullet}{-}O^{-} \leftrightarrow U^{IV}{-}O{\equiv}C{-}O^{-}$. In these charge-separated resonance structures, the uranium center is oxidized to uranium(IV) and the CO_2 ligand reduced by one electron.

Carbon dioxide has been implicated as a main contributor to global warming because of its role in radiative forcing (*1*). However, CO_2 also represents an abundant renewable resource for the production of fine chemicals and clean fuels. Interest in metal-mediated multielectron reduction of CO_2 therefore remains high, but the molecule's inherent thermodynamic stability hinders the development of metal catalysts that achieve CO_2 activation and functionalization.

Particularly intriguing for synthetic chemists is the discovery of relatively simple coordination complexes that bind CO_2 and facilitate its reduction (*2*). Chemists have isolated and structurally characterized several synthetic metal complexes of CO_2, such as Aresta's archetypal [$(Cy_3P)_2Ni(CO_2)$] (Cy = cyclohexyl) (*3*, *4*) and Herskowitz's [$(diars)_2M(CO_2)(Cl)$] [diars = *o*-phenylenebis(dimethylarsine); M = Ir, Rh] (*5*), featuring the bidentate η^2-**CO**O and carbon-bound η^1-**C**O_2 binding modes, respectively. Activation of CO_2 via its adsorption on metal surfaces is of considerable interest for catalysis at the gas-surface interface (*6*, *7*). Most recently, Andrews and co-workers studied the interaction of CO_2 with a variety of transition (*8*) and actinide (*9*) metal atoms generated via laser ablation. Although C–O bond cleavage of a proposed intermediate η^2-**CO**O complex is predominant in these surface-adsorbed systems, there also is spectral evidence for η^1-**O**CO adsorption in low-temperature matrices (Scheme 1) (*8*). The most important CO_2 activation process occurs naturally during photosynthesis. It was proposed that during photosynthetic CO_2 fixation, an oxygen-coordinated CO_2 ligand (η^1-**O**CO) is enzymatically reduced by ribulose-1,5-bisphosphate carboxylase-oxygenase (RuBisCO) (*10*). Oxygen coordination appears to be an indispensable step for C-functionalization in this system. Recently, the relevance of the η^1-**O**CO coordination mode for biological systems was fueled by a crystallographic study on a deacetoxycephalosporin C synthase (DAOCS) mutant. The presence of electron density in proximity to the active site's iron center was found to be consistent with a monodentate O-bound CO_2 molecule (*11*). However, definitive structural characterization of inorganic coordination complexes with a linear oxygen-bound η^1-**O**CO coordination mode has remained elusive (*2*).

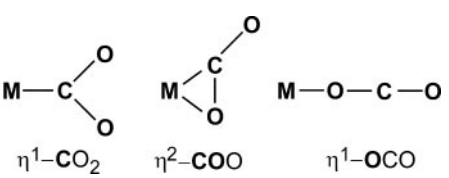

Scheme 1.

Department of Chemistry and Biochemistry, University of California, San Diego, 9500 Gilman Drive, MC 0358, La Jolla, CA 92093, USA.

*To whom correspondence should be addressed. E-mail: kmeyer@ucsd.edu

The large negative reduction potential and oxophilicity of trivalent uranium complexes can be applied to CO_2 fixation. Coordination complexes of uranium have undergone a renaissance in the past few years (*12*). It has been shown that, if stabilized by a suitable supporting ligand set, uranium compounds are highly reactive (*13*) and can engage in the formation of carbon monoxide (*14*, *15*), dinitrogen (*16*, *17*), and even alkane complexes through *f*-orbital interaction (*18*).

Here, we report carbon dioxide coordination by a uranium compound resulting in reductive activation of the CO_2 ligand. For the exploration of CO_2 coordination and redox chemistry with a reactive uranium center, we sought to use the electron-rich uranium(III) complex [$((^{Ad}ArO)_3tacn)U^{III}$] [**1**, $(^{Ad}ArOH)_3tacn$ = 1,4,7-tris(3-adamantyl-5-*tert*-butyl-2-hydroxybenzyl)1,4,7-triazacyclononane] (*19*).

The uranium center of coordinatively unsaturated **1** is located deep inside a cavity formed by the hexadentate aryloxide-functionalized polyamine chelator. Intramolecular hydrophobic interactions between the hydrocarbyl substituents displace the U ion below the trigonal plane of the three aryloxide ligands. The sterically demanding adamantyl groups form a narrow cylindrical cavity above the uranium ion, thereby providing restricted access to an incoming ligand and protecting the uranium center from bimolecular decomposition reactions.

Exposure of toluene solutions or even solid samples of intensely colored **1** to CO_2 gas (1 atm) results in instantaneous discoloration of the samples (*20*). After filtration and concentration of the toluene reaction mixture, colorless crystals of [$((^{Ad}ArO)_3tacn)U^{IV}(CO_2)$] (**2**) are isolated in ~50% yield (Scheme 2). The infrared spectrum of the crystalline sample in Nujol clearly exhibits a distinct vibrational band centered at 2188 cm^{-1}, indicative of a coordinated and significantly activated CO_2 ligand. When **1** is exposed to isotopically labeled $^{13}CO_2$ gas, this band shifts to 2128 cm^{-1} (fig. S1). The $^{12}C/^{13}C$ isotopic ratio *R* (2188/2128) of 1.0282 is close to that of free CO_2 gas (*R* = 1.0284), indicative of a molecule that has the linear geometry of free CO_2 as well as the same carbon motion, $\nu_3(\nu_{as}OCO)$, in this vibrational mode.

An x-ray diffraction analysis of single crystals obtained from a mixture of methylene chloride and diethyl ether confirms the presence of a coordinated carbon dioxide ligand (*21*). Unexpectedly, the CO_2 ligand in [$((^{Ad}ArO)_3tacn)U^{IV}(CO_2)$] · 2.5 Et_2O (**2** · 2.5 Et_2O) is coordinated to the uranium ion in a linear, oxygen-bound η^1-**O**CO fashion (Fig. 1). This CO_2 coordination mode likely is enforced by the adamantyl substituents of the supporting ligand platform. The U−OCO group has a U−O bond length of 2.351(3) Å (here and below, values in parentheses are errors in the last significant digit); the neighboring C–O bond length is 1.122(4) Å; and the terminal C−O bond length is 1.277(4) Å. The U−O−C and O−C−O angles of 171.1(2)° and 178.0(3)°, respectively, are close to linear. These metric parameters, together with the frequency redshift of the vibrational bands (ν_3:$\nu_{O}{}^{12}{}_{CO}$ = 2188 cm^{-1}, $\nu_{O}{}^{13}{}_{CO}$ = 2128 cm^{-1}), strongly suggest a molecular structure with charge-separated resonance structures $U^{IV}{=}O{=}C^{\bullet}{-}O^{-} \leftrightarrow U^{IV}{-}O{\equiv}C{-}O^{-}$. Such an electronic structure would result from a metal-centered one-electron oxidation upon CO_2 coordination.

This bonding assignment is further supported by comparison of complex **2** with a structurally similar azido complex (Fig. 2). Uranium(III) complex **1** reacts with one-electron oxidizers, such as trimethylsilyl azide (*22*), benzyl chloride, benzyl bromide, and iodine to form the respective seven-coordinate halide and pseudohalide U^{IV} complexes [$((^{Ad}ArO)_3tacn)U^{IV}(X)$] [X = N_3 (**3**), Cl, Br, I] (*20*). The azido ligand, which typically adopts a bent orientation at metal centers, is linearly coordinated in complex **3** [$\angle(U{-}N^{\alpha}{-}N^{\beta})$ = 175.6(3)°, $\angle(N^{\alpha}{-}N^{\beta}{-}N^{\gamma})$ = 177.2(5)°, *d* (U−N^{α}) = 2.372(3) Å, *d* ($N^{\alpha}{-}N^{\beta}$) = 1.128(4) Å, *d* ($N^{\beta}{-}N^{\gamma}$) = 1.147(5) Å] (*21*). As with the CO_2 coordination mode in **2**, this bonding motif is most likely imposed by the sterically encumbering substituents. The azido ligand allows estimation of the cavity depth of the supporting ligand framework, which is approximately equal to the sum of the *d* (U−N) and *d* (N−N) bond distances (4.65 Å).

Comparison of the CO_2 and azido complexes **2** and **3** with the starting compound **1** reveals that after axial ligand coordination, the central uranium ion is situated closer to the trigonal planar aryloxide ligand environment. Whereas the uranium(III) ion in **1** is located 0.88 Å below the ligand plane, the uranium center in **2** and **3** is displaced only 0.274 Å and 0.291 Å below the plane, respectively. The average U−N_{tacn} and U−O_{ArO} distances in **3** were determined to be 2.659(3) and 2.155(2) Å and thus are almost identical to those found in **2** [2.673(2) and 2.157(2) Å]. The U−O_{ArO} bond distances in **2** and **3** are significantly shorter than those found in the parent trivalent complex **1** [2.226(9) Å], as well as U^{III} complexes of the related ($^{t\text{-}Bu}$ArO)tacn ligand system (*23*), namely [$((^{t\text{-}Bu}ArO)_3tacn)U^{III}(CH_3CN)$] [2.265(5) Å] (*22*) and [$((^{t\text{-}Bu}ArO)_3tacn)U^{III}(^{Me}Cy\text{-}C6)$] [2.244(3) Å] (*18*). Given the assignment of the valence in **3** as U^{IV} with an N_3^- azido ligand and the structural similarities of complexes **2** and **3**, the oxidation state for the uranium center in **2** is also assigned as U^{IV} with a CO_2^- ligand.

The electronic structure of **2** was examined by comparison of superconducting quantum in-

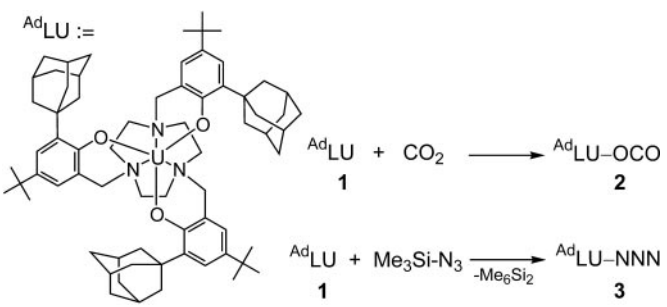

Scheme 2. Synthesis of complexes.

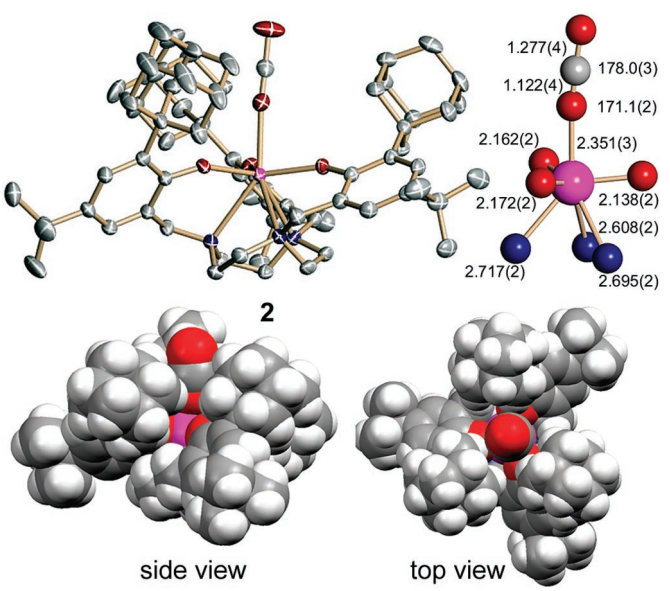

Fig. 1. ORTEP (Oak Ridge thermal ellipsoid plot) of uranium CO_2 complex **2** and in crystals of **2** · 2.5 Et_2O (top left) with core structure and metric parameters in angstroms and degrees (top right) and space-filling representations (bottom). Uranium, magenta; nitrogen, blue; oxygen, red; carbon, gray.

terference device (SQUID) magnetization data and electronic absorption spectra of **1**, **2**, and **3** (*20*). Over the temperature range 5 to 300 K, solid samples of **2** display a distinctly temperature-dependent magnetic moment (Fig. 3).

The magnetic moment μ_{eff} of **2** was determined to be 2.89 μ_B (where μ_B is in units of Bohr magnetons) at 300 K; it slowly decreases with decreasing temperatures, reaching a value of 2.6 μ_B at 100 K. Below 100 K, μ_{eff} decreases rapidly, reaching a value of 1.51 μ_B at 5 K. Between 300 K and 75 K, the temperature dependence of the μ_{eff} value of **2** shows a curvature reminiscent of data obtained for the U^{IV} complex **3**. Although the room-temperature μ_{eff} value of **2** is close to that found for the azide complex **3**, the low-temperature value is similar to that of the U^{III} (f^3) starting material **1** (1.73 μ_B at 5 K), which has a doublet ground state at low temperatures (*19*). Generally, U^{IV} complexes with an f^2 ($^3H_4$) electron configuration have a singlet ground state that exhibits temperature-independent paramagnetism at very low temperatures, resulting in μ_{eff} values of ~0.5 μ_B like that of **3** (fig. S2) (*20*). The CO_2 complex **2**, however, has a significantly greater μ_{eff} value at low temperature, which reinforces the description of the CO_2 ligand as one-electron reduced $CO_2^{\bullet-}$ radical anion coordinated to a U^{IV} ion. The transferred charge (virtually one unpaired electron) is localized on the coordinating CO_2 ligand. In contrast to the closed-shell N_3^- ligand of **3**, the open-shell $CO_2^{\bullet-}$ likely contributes to the observed increase in μ_{eff} value of **2** at low temperatures.

To further probe the formal oxidation state of the uranium ion, we recorded the ultraviolet/visible/near-infrared (NIR) electronic absorption spectrum of **2** and compared it to spectra of known U^{III} and U^{IV} complexes (figs. S3 and S4) (*20*). Most notably, although U^{III} and U^{V} complexes of the $(ArO)_3$tacn ligand are deeply colored (*22*), U^{IV} complexes of this ligand system, as well as the uranium-CO_2 complex **2**, appear colorless to very pale blue-green in solution and in the solid state (*22*, *23*). The absorption spectra of deep red uranium(III) complexes of the $((ArO)_3$tacn)U system, such as **1**, are dominated by an intense absorption band centered at 455 nm (ε = 1945 M^{-1} cm^{-1}) (*20*), which can be assigned to either an allowed $d-f$ ligand field or ligand-to-metal charge-transfer transition. In addition, $f-f$ transitions give rise to a number of weak absorption bands in the NIR region between 800 and 2200 nm (ε = 50 to 150 M^{-1} cm^{-1}). In contrast, the colorless uranium(IV) complexes $[((ArO)_3tacn)U(CO_2)]$ (**2**) and $[((ArO)_3tacn)U(N_3)]$ (**3**) exhibit weak absorption bands over the entire visible and NIR region (*20*). The band intensities and positions are characteristic of the U^{IV} f^2 ion (*24*). Taken together, the metrical and spectroscopic data thus support a one-electron transfer from U to CO_2 in formation of this linearly bound, O-coordinated complex.

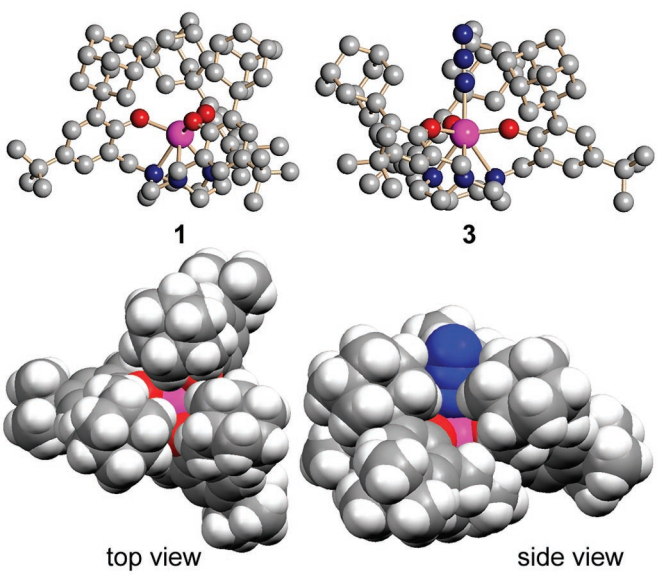

Fig. 2. Molecular structure of precursor complex **1** in crystals of **1** · C_6H_{14} (top left) and azido complex **3** in crystals of **3** · 3 CH_2Cl_2 (top right) and respective space-filling representations (bottom).

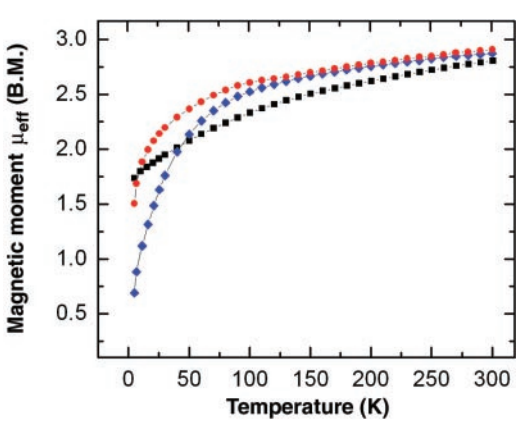

Fig. 3. Temperature-dependent SQUID magnetization data for trivalent **1** (■), uranium CO_2 complex **2** (●), and tetravalent azido complex **3** (◆) measured in the temperature range 5 to 300 K at 1 T.

References and Notes

1. P. Falkowski *et al.*, *Science* **290**, 291 (2000).
2. D. H. Gibson, *Chem. Rev.* **96**, 2063 (1996).
3. M. Aresta, C. F. Nobile, V. G. Albano, E. Forni, M. Manassero, *J. Chem. Soc. Chem. Commun.* **1975**, 636 (1975).
4. M. Aresta, C. F. Nobile, *J. Chem. Soc. Dalton Trans.* **1977**, 708 (1977).
5. T. Herskovitz, *J. Am. Chem. Soc.* **99**, 2391 (1977).
6. H. J. Freund, R. P. Messmer, *Surf. Sci.* **172**, 1 (1986).
7. D. H. Gibson, *Coord. Chem. Rev.* **185–186**, 335 (1999).
8. P. F. Souter, L. Andrews, *J. Am. Chem. Soc.* **119**, 7350 (1997).
9. L. Andrews, M. F. Zhou, B. Y. Liang, J. Li, B. E. Bursten, *J. Am. Chem. Soc.* **122**, 11440 (2000).
10. H. Mauser, W. A. King, J. E. Gready, T. J. Andrews, *J. Am. Chem. Soc.* **123**, 10821 (2001).
11. H. J. Lee *et al.*, *J. Mol. Biol.* **308**, 937 (2001).
12. D. L. Clark, A. P. Sattelberger, R. A. Andersen, *Inorg. Synth.* **31**, 307 (1997).
13. P. L. Diaconescu, P. L. Arnold, T. A. Baker, D. J. Mindiola, C. C. Cummins, *J. Am. Chem. Soc.* **122**, 6108 (2000).
14. J. G. Brennan, R. A. Andersen, J. L. Robbins, *J. Am. Chem. Soc.* **108**, 335 (1986).
15. M. del Mar Conejo *et al.*, *Chem. Eur. J.* **5**, 3000 (1999).
16. P. Roussel, P. Scott, *J. Am. Chem. Soc.* **120**, 1070 (1998).
17. A. L. Odom, P. L. Arnold, C. C. Cummins, *J. Am. Chem. Soc.* **120**, 5836 (1998).
18. I. Castro-Rodriguez *et al.*, *J. Am. Chem. Soc.* **125**, 15734 (2003).
19. H. Nakai, X. Hu, L. N. Zakharov, A. L. Rheingold, K. Meyer, *Inorg. Chem.* **43**, 855 (2004).
20. See supporting material on *Science* Online.
21. Data collections were performed at 100(2) K on a Bruker SMART APEX diffractometer with a charge-coupled device (CCD) area detector, with graphite-monochromated Mo Kα radiation (λ = 0.71073 Å). Molecular structures were solved by direct methods and refined on F^2 by full-matrix least-squares techniques. For **2** · 2.5 Et_2O: monoclinic, $P2_1/n$, a = 16.0494(12) Å, b = 21.0575(16) Å, c = 22.2629(17) Å, β = 93.3720(10), V = 7510.9(10) Å^3, Z = 4, R = 0.0326, $wR2$ = 0.0772. For **3** · 3 CH_2Cl_2: orthorhombic, $P2_12_12_1$, a = 10.7294(6) Å, b = 23.0272(13) Å, c = 28.5498(17) Å, V = 7053.7(7) Å^3, Z = 4, R = 0.0529, $wR2$ = 0.1191.
22. I. Castro-Rodriguez, K. Olsen, P. Gantzel, K. Meyer, *J. Am. Chem. Soc.* **125**, 4565 (2003).
23. I. Castro-Rodriguez, K. Olsen, P. Gantzel, K. Meyer, *Chem. Commun.* **2002**, 2764 (2002).
24. J. J. Katz, L. R. Morss, G. T. Seaborg, *The Chemistry of the Actinide Elements* (Chapman & Hall, New York, 1980).

25. Supported by the University of California, San Diego, and U.S. Department of Energy grant DE-FG02-04ER15537. We thank W. L. S. Andrews and N. Edelstein for insightful discussions and NIH for a fellowship to I.C.R. (3 T32 DK07233-2651). K.M. is an Alfred P. Sloan fellow. Crystallographic data were deposited in the Cambridge Crystallographic Database Centre (**2**: CCDC-244303; **3**: CCDC-244304).

Supporting Online Material

www.sciencemag.org/cgi/content/full/305/5691/1757/DC1
Materials and Methods
SOM Text
Figs. S1 to S4

9 July 2004; accepted 13 August 2004